THE ASTROPHYSICAL JOURNAL, 448:281–288, 1995 July 20

THE SYNCHROTRON SELF-COMPTON MODEL FOR X-RAY AND γ-RAY EMISSION FROM PULSARS

K. S. CHENG[1] AND D. M. WEI[1,2]
Received 1994 November 7; accepted 1995 January 30

ABSTRACT

We compare the observed X-ray luminosity emitted from pulsars with that calculated from various theoretical models and find that the X-ray emission from six pulsars is much stronger than that predicted by theoretical models. We suggest that these pulsars with unusually intense X-ray emission could also be γ-ray emitters. Electrons/positrons are accelerated in the outer magnetospheric gap and lose most of their energy via curvature radiation (primary photons), which will be converted to secondary $e^{\pm}$ pairs outside the gap in collision with the secondary X-rays. A simple synchrotron self-Compton model is then used to calculate the X-ray and γ-ray emission from the secondary $e^{\pm}$ pairs. This model only contains a single free parameter, which characterizes the size of the acceleration region and can be estimated by comparison with that of the Crab pulsar. Our model results are consistent with the observed data and upper limits of γ-ray emission and phase separation between pulses. Other implications for future observations are also discussed in the text.

Subject headings: elementary particles — gamma rays: theory — pulsars: general — radiation mechanisms: nonthermal — stars: neutron — X-rays: stars

1. INTRODUCTION

Up to now, nearly 600 pulsars have been reported, most in the radio band (Taylor, Manchester, & Lyne 1993). However, high-energy emissions have been detected only from a very small fraction of pulsars. Since the launch of the *Compton Gamma Ray Observatory*, only six pulsars have been identified as γ-ray pulsars; they are the Crab (Nolan et al. 1993; Wilson et al. 1993), Vela (Strickman et al. 1993), Geminga (Mattox et al. 1992; Bertsch et al. 1992), PSR 1706−44 (Thompson et al. 1992), PSR 1509−58 (Wilson et al. 1993; Ulmer et al. 1993), and PSR 1055−52 (Fierro et al. 1993). In addition to radio and γ-ray emission, some rotation-powered pulsars have also been detected as X-ray pulsars; there are now 15 pulsars that have been confirmed as nonaccreting X-ray pulsars (cf. Ögelman 1993; Becker & Trümper 1993). It is very interesting to note that the the six γ-ray pulsars are all X-ray pulsars. In fact, this is consistent with theoretical γ-ray pulsar models (Harding 1981; Cheng, Ho, & Ruderman 1986a, b), in which either thermal X-rays resulting from polar cap heating by the return current or nonthermal X-rays as the tail of synchrotron radiation of secondary $e^{\pm}$ pairs will be emitted from pulsars.

According to the outer gap model (Cheng et al. 1986a, b, hereafter CHR I and CHR II), optical photons to hard X-rays (eV to MeV) of the Crab pulsar are emitted by secondary $e^{\pm}$ pairs, which are created outside the accelerating regions (outer gap) via synchrotron radiation. But soft γ-rays to high-energy γ-rays (MeV to 10 GeV) are produced by inverse Compton scattering between synchrotron photons (1 eV to MeV) and the secondary $e^{\pm}$ pairs which are these pairs radiating the synchrotron photons. These synchrotron self-Compton mechanisms, in fact, also appear in the Crab Nebula (Gould 1965; Rieke & Weekes 1969; Kennel & Coroniti 1984; De Jager & Harding 1992).

We want to point out that it is very difficult to determine a unique spectrum by using *ROSAT* data because the absorption of the interstellar medium in the energy range of *ROSAT* is quite strong. In many cases (e.g., PSR J0437−4715; cf. Becker & Trümper 1993), it is very difficult to differentiate a power spectrum from a thermal spectrum by the data. In this paper, we first assume that X-rays from pulsars are thermal X-rays and then test whether this assumption is consistent with the theoretical models. For those pulsars with unusually intense X-rays, in other words, the observed X-ray intensity is higher than that predicted by theoretical thermal X-ray models. We will investigate whether these X-rays can be emitted from the outer magnetospheric gap in terms of synchrotron self-Compton mechanisms. Furthermore, we can use the X-ray emission to predict the γ-ray intensity from these pulsars. In § 2, we review a Crab-type outer gap model. In § 3, we review some conventional X-ray emission models for pulsars, then we compare the X-ray intensity predicted by these models to the observed data in order to identify the unusually intense X-ray emitters. In § 4, we present the synchrotron self-Compton model and estimate the maximum energy and the energy distribution of the secondary $e^{\pm}$ pairs and the total power of radiation. Finally, we apply our model to pulsars with unusually intense X-ray emission to predict their X-ray and γ-ray spectra in § 5.

2. RADIATION MECHANISMS OF CRAB-TYPE PULSARS

The CHR model assumed that a global current flow pattern through the magnetosphere of a spinning magnetized neutron star results in large regions of magnetospheric charge depletion. This would result in a large electric field along the magnetic field lines in these regions which can accelerate primary electrons/positrons to extremely relativistic energies. The total potential of this accelerator can be expressed as

$$\Delta V = 6 \times 10^{12} f^2 B_{12} P^{-2} \text{ V}, \quad (1)$$

and the rate of particles passing through the gap is

$$\dot{N} = 2.5 \times 10^{30} f B_{12} P^{-2} \text{ s}^{-1}, \quad (2)$$

where f is the fractional volume of the outer magnetosphere occupied by the outer gap. However, the primary electrons/

[1] Department of Physics, University of Hong Kong, Pokfulam Road, Hong Kong.
[2] Department of Astronomy, Nanjing University, Nanjing, P.R. China

positrons accelerated inside the gap cannot achieve the energy of the full potential of the gap, due to the loss of curvature radiation. The typical energy of the curvature photon is given by

$$E_{\rm cur} \simeq 10^8 f^{3/2} P^{-7/4} B_{12}^{3/4} \text{ eV} . \quad (3)$$

These curvature photons will convert to secondary $e^{\pm}$ pairs in collision with the X-rays which are radiated by the same secondary $e^{\pm}$ pairs via synchrotron radiation. These secondary pairs can prevent the further growth of the outer gap. Inverse Compton scattering of secondary $e^{\pm}$ on the same X-rays boosts a significant fraction of X-rays to γ-rays. The observed X-rays and γ-rays from the Crab pulsar are a combination of secondary synchrotron radiation and inverse Compton scattering. This type of synchrotron self-Compton mechanism is very common in other astrophysical objects, e.g., the Crab Nebula, active galactic nuclei, etc.

In principle, the parameter f can be determined by this model self-consistently. If every pulsar has the same angle between its magnetic axis and rotation axis, f can be scaled from that of the Crab pulsar (CHR II, eq. [6.7]):

$$f \simeq 0.1 \left(\frac{B}{B_{\rm Crab}}\right)^{-39/60} \left(\frac{P}{P_{\rm Crab}}\right)^{99/60} , \quad (4)$$

and a Crab-type pulsar should have a period

$$P \leq 5 \times 10^{-2} B_{12}^{2/5} , \quad (5)$$

which is obtained by equating the efficiency of a Crab-type pulsar and that of a Vela-type (Cheng & Ding 1994). Chen & Ruderman (1993) point out that the inclination will play a crucial role in pulsar evolution. If the mean distance to the outer gap in Geminga is changed by a factor 2, it can no longer be a γ-ray pulsar. Due to this uncertainty, we will treat f as a free parameter in our calculation presented in § 4. But the value of f is expected to be around the value given by equation (4). For this reason, a pulsar with period larger than that given in equation (5) may still be a Crab-type pulsar as long as its inclination angle is larger than that of the Crab pulsar. Then the mean magnetic field in the outer gap could be the same as that of the Crab pulsar such that Crab-type mechanisms may still be important. Finally, we want to emphasize that nonthermal intense X-ray emission is one of the key features of Crab-type radiation mechanisms.

3. THERMAL X-RAY EMISSION FROM PULSARS

There are five possible mechanisms to cause thermal X-ray emission from pulsars. Pulsars are expected to be born with extremely high temperature ($\sim 10^{10}$ K); their temperature will be cooled via neutrino emission and blackbody radiation. For pulsars of age $\geq 10^3$ yr, their core temperature is given by (cf. Cheng et al. 1992)

$$T_c = 2.1 \times 10^8 (M_{\rm cr}/M)/0.05]^{-1/4} \rho_{14}^{1/12} t_3^{-1/4} \text{ K} , \quad T > T_a , \quad (6)$$

or

$$T_c = 1.8 \times 10^7 t_5^{-5} g_{s14}^{-5} M_*^5 \rho_{14}^{5/3} \text{ K} , \quad T < T_a , \quad (7)$$

where $T_a = 1.3 \times 10^8 [(M_{\rm cr}/M)/0.05]^{-0.263} g_{s14}^{0.263}$ K, $M_{\rm cr}$ is the mass of the stellar crust, M_* is the mass of the star in units of one solar mass, ρ_{14} is the mean density of the star in units of 10^{14} g cm^{-3}, t_q is time in units of q yr, and g_{s14} is the surface gravity in units of 10^{14} cm s^{-2}. The surface temperature and the core temperature are simply related by (Gudmundson, Pethick, & Epstein 1982)

$$T_c = 1.3 \times 10^8 \left(\frac{T_{s6}^4}{g_{s14}}\right)^{0.455} \text{ K} , \quad (8)$$

where T_{s6} is the surface temperature in units of 10^6 K. The thermal X-ray luminosity due to pure neutron star cooling without heating is simply given by

$$L_{\rm cool} = 4\pi R^2 \sigma T_s^4 . \quad (9)$$

On the other hand, there are at least four possible heating mechanisms due to the internal and magnetospheric activities of pulsars.

3.1. *Internal Heating Mechanisms*

It is commonly accepted that neutron superfluid exists in the inner crust of neutron stars. The rotating superfluid will form quantized vortex lines. In fact, the superfluid velocity is completely determined by the distribution of vortex lines. The vortex lines are energetically favorable to pinning in the nuclei of the solid. As the pulsar spins down due to the dipole radiation, the superfluid cannot respond because the distribution of the vortex lines is fixed by the lattice until the velocity lag between the superfluid and the solid (the vortex lines) is so large that the Magnus force, which is proportional to the velocity lag, is strong enough to reduce the pinning barrier. In this case, the thermal activation can produce a steady creep velocity for the vortex lines in the direction of the Magnus force, and the velocity lag is maintained as a constant. This process is a frictional interaction between the crust and the superfluid which dissipates the free energy of the crustal neutron superfluid differential rotation. The heat produced by this process is given by (Alpar et al. 1984; Shibazaki & Lamb 1989)

$$L_f = I_p \omega_{\rm cr} \dot{\Omega} \equiv \beta \dot{\Omega} , \quad (10)$$

where I_p is the moment of inertia of neutron superfluid, $\omega_{\rm cr}$ is the critical angular velocity lag, beyond which the Magnus force becomes larger than the pinning force which keeps vortex lines at the nuclei, and $\dot{\Omega}$ is the spin-down rate of angular velocity. I_p could be ranging from over 20% (very stiff equation of state; i.e., Pandharipande, Pines, & Smith 1976) to less than 1% (soft equation of state; i.e., Baym, Pethick, & Sutherland 1971) of the total moment of inertia of the star. Detailed analyses of the postglitch relaxation curves of nine Vela glitches and six Crab glitches (Alpar et al. 1993, 1994) indicate that I_p is less than 10% of total stellar moment inertia, which favors a moderately stiff equation of state (e.g., Wiringa & Fiks 1988). The value of $\omega_{\rm cr}$ can also range from 0.1 (superweak pinning; cf. Alpar et al. 1984) to 10 (strong pinning region; cf. Epstein & Baym 1988). However, both postglitch relaxation (Alpar et al. 1993, 1994) and X-ray observations of nearby pulsars (Alpar et al. 1987) prefer a small value of $\omega_{\rm cr}$. So, we shall assume $\beta \simeq 10^{43}$ ergs s.

Another possible internal heating mechanism is crust cracking. As the pulsar spins down, the stellar configuration will deviate from its equilibrium configuration, which depends on the angular velocity of the star, due to the finite rigidity of the solid. The stress will increase until it reaches some critical value $\sigma_c = \mu\theta_c$, where μ is the shear modulus and θ_c is the maximum (critical) shear angle before fracture. Strain energy will be released in crust cracking; it is estimated that the power released

is given by (Cheng et al. 1992)

$$L_{cr} = 2B\theta_c^2 \dot{\Omega}/\Omega , \quad (11)$$

where B is a constant to describe the strength of the crust (Baym & Pines 1971) which depends on the equation of state and the value of θ_c ranges from 10^{-2} for an ideal Coulomb lattitice to 10^{-4} for a dislocation-dominated lattice (Ruderman 1991). Chong & Cheng (1993) used L_{cr} to compare with X-ray observations of old pulsars and concluded that $\theta_c \sim 10^{-2}$ for a moderately stiff equation of state which also gives $B \simeq 10^{48}$ ergs.

3.2. *Magnetospheric Heating Mechanisms*

Both coherent radio waves and γ-rays are expected to be emitted by relativistic electrons/positrons which are accelerated by electrostatic accelerators located either above the polar cap or near the null charge surface where $\boldsymbol{\Omega} \cdot \boldsymbol{B} = 0$. A good fraction of these relativistic electrons/positrons will stream back to the neutron star and heat up the surface, which causes the emission of thermal X-rays. According to polar gap model by Ruderman & Sutherland (1975), the primary electrons/positrons can obtain $7 \times 10^{30} s_6^{4/7} P^{-15/7} B_{12}^{6/7}$ ergs s^{-1} from the polar gap. However, Arons and his coworkers (Arons & Scharlemann 1979; Scharlemann, Arons, & Fawley 1978) show that no more than 10% of oppositely charged primary particles can return to the surface because of oppositely charged particles are produced near the polar gap boundary where the electric field is not strong enough to return all oppositely charged particles. Therefore, the X-ray luminosity produced by the return current is given by

$$L_p \simeq 7 \times 10^{29} \alpha_{-1} s_6^{4/7} P^{-15/7} B_{12}^{6/7} \text{ ergs s}^{-1} , \quad (12)$$

where α_{-1} is the fraction of oppositely charged primary electrons/positrons that can return to the stellar surface in units of 0.1, s_6 is the radius of curvature in units of 10^6 cm, P is the rotation period, and B_{12} is the surface magnetic field in units of 10^{12} G.

Another possible source of return current is the outer magnetospheric gap (CHR I and II), where electrons/positrons can also be accelerated to extremely relativistic energies. After leaving the outer gap, half of these primary electrons/positrons will move toward the star and eventually strike the stellar surface. Although most of the energy of the primary particles will be lost on the way to the star via curvature radiation, Halpern & Ruderman (1993) estimate that $16P^{1/3}$ ergs per particle will still remain and eventually deposit on the stellar surface. This energy will be emitted in terms of thermal X-rays, and the luminosity is

$$L_{out} \simeq 4 \times 10^{30} (f/0.3) B_{12} P^{-5/3} \text{ ergs s}^{-1} , \quad (13)$$

where f is the fractional volume of outer magnetosphere occupied by the outer gap. The parameter is estimated to be 0.2 for the Vela pulsar and 0.7 for Geminga (Cheng 1994). In Table 1, we have assumed $f/0.3 = 1$.

3.3. *Comparison with Observed X-Rays from Pulsars*

In Table 1, we compare the observed X-ray luminosity with various theoretical thermal X-ray models, which we have discussed in previous subsections. We can see that the observed X-ray emission is consistent with the theoretical models to within a factor of 3, except for PSR 0531+21, PSR 0540−69, PSR 1509−58, PSR 1951+32, PSR 1823−13, and PSR 2334+61. The magnetic fields of the first four pulsars show that their periods are still close to that given in equation (5). Therefore, they should be Crab-like pulsars. The last two pulsars have periods larger than that in equation (5) by at least a factor of 2. It appears that they should not be Crab-like pulsars unless their inclination angles are significantly larger than that of the Crab pulsar. In fact, the X-ray observations seem to suggest that they are Crab-like pulsars.

4. SYNCHROTRON SELF-COMPTON MODEL

The steady state energy distribution of the $e^{\pm}$ pairs is expected to be

$$\frac{dN(E_e)}{dE_e} = N_0 E_e^{-\alpha} , \quad E_{min} \le E_e \le E_{max} , \quad (14)$$

where E_e is the electron energy, $N_0 \approx \dot{N}/\Omega$, and the power index α, low energy cutoff E_{min}, and upper energy cutoff E_{max} can be estimated by the following arguments. Using the Crab-type mechanisms described in § 2, we can approximate the primary γ-ray spectrum, which is curvature radiation by monoenergetic electrons/positrons, by

$$\frac{d^2 N_p(E_\gamma)}{dE_\gamma dt} \simeq e\dot{N} \Delta V \delta(E_\gamma - E_{cur}) , \quad (15)$$

where $\dot{N}$, ΔV, and E_{cur} are given by equations (1)–(3). Let us assume that the Crab-type optical depth is large, then all these

TABLE 1

X-RAY EMISSION FROM PULSARS

PSR	P	B_{12}	log L_x^{obs}	log L_{cr}	log L_f	log L_p	log L_{out}
0531+21.....	0.033	3.8	36.0	33.5	34.4	32.4	33.65
0540−69.....	0.05	5.0	36.3	33.2	34.1	32.3	33.47
1509−58.....	0.15	15.5	34.3	32.6	33.0	31.45	32.8
0833−45.....	0.089	3.4	32.7	32.6	33.0	31.45	32.8
1951+32.....	0.04	0.49	33.4	32.6	32.4	30.5	32.6
1706−44.....	0.102	3.1	32.0	32.4	32.7	31.25	32.7
1823−13.....	0.101	2.3	33.9	32.3	32.5	31.0	32.6
2334+61.....	0.495	9.8	33.0	31.3	31.7	30.9	32.1
0656+14.....	0.385	4.7	32.5	31.3	31.4	30.5	32.0
0630+18.....	0.237	1.6	31.7	31.4	31.1	30.0	31.8
1055+52.....	0.197	1.1	32.5	31.4	31.0	29.8	31.8
1929+10.....	0.227	0.51	29.0	31.0	30.1	29.0	31.4
0950+08.....	0.229	0.245	29.0	30.7	29.5	28.3	31.0
J0437−47.....	0.00575	0.0008	30.8	32	27	29.3	31.2

NOTE.—The X-ray data is summarized by Ögelman 1993, except PSR J0437−47 which is obtained from Becker & Trümper 1993.

primary photons will convert to be secondary $e^{\pm}$ pairs with the following spectrum (Blumenthal & Gould 1970):

$$\frac{dN(E_e)}{dE_e} = N_0 E_e^{-2} . \quad (16)$$

It is clear that the upper energy cutoff is given by

$$E_{\max} \simeq \frac{E_{\rm cur}}{2} . \quad (17)$$

On the other hand, the lower energy cutoff can be determined by physical processes. For synchrotron radiation, the energy loss rate is

$$\dot{\gamma}_{\rm syn} = \frac{2e^2\omega_B^2\gamma^2}{3mc^3} , \quad (18)$$

where $\omega_B = eB \sin\theta/mc$ is the cyclotron frequency, $\sin\theta$ is the mean pitch angle of the secondary pairs (since the fractional size of the secondary region is f, we can approximate $\sin\theta \sim f$), γ is the Lorentz factor, m is the electron mass, and c is speed of light. Approximately, we have

$$\frac{\gamma}{\dot{\gamma}_{\rm syn}} \sim \frac{r}{c} , \quad (19)$$

where $r = \beta r_L$ represents the distance to the emission region and $r_L = c/\Omega$ is the light cylinder radius. So we can obtain

$$\gamma_{\rm min}^{\rm syn} \sim \frac{mc^2}{r\sigma_{\rm T}\epsilon_B} , \quad (20)$$

with $\epsilon_B = B^2/4\pi$ and $\sigma_{\rm T}$ the Thomson cross section. Similarly, the energy loss rate due to inverse Compton scattering is

$$\dot{\gamma}_{\rm ICS} \sim \frac{\gamma^2\sigma_{\rm T}\epsilon_{\rm syn}}{mc} , \quad (21)$$

where

$$\epsilon_{\rm syn} \simeq \frac{F_{\rm syn}E_c}{cr^2\Delta\Omega} \quad (22)$$

is the energy density of synchrotron radiation. $F_{\rm syn}$ is the X-ray/soft γ-ray flux, E_c is the characteristic energy of synchrotron photons, and $\Delta\Omega$ is the solid angle. We also have

$$\frac{\gamma_{\rm ICS}}{\dot{\gamma}_{\rm ICS}} \sim \frac{r}{c} , \quad (23)$$

so

$$\gamma_{\rm min}^{\rm ICS} \sim \frac{mc^2}{r\sigma_{\rm T}\epsilon_{\rm syn}} . \quad (24)$$

So, we obtain

$$E_{\rm min} = \max(1, \gamma_{\rm min})mc^2 \quad (25)$$

where $\gamma_{\rm min} = \min(\gamma_{\rm min}^{\rm syn}, \gamma_{\rm min}^{\rm ICS})$.

Having the electron energy distribution, we can calculate the synchrotron radiation spectrum

$$F_{\rm syn}(E_\gamma) = \frac{3^{1/2}e^3B(r)}{mc^2h}\int_{E_{\rm min}}^{E_{\max}}\frac{dN(E_e)}{dE_e}\frac{F(x)}{E_\gamma}dE_e , \quad (26)$$

where h is the Planck constant, $x = E_\gamma/E_c$, and

$$E_c = \frac{3}{2}\left(\frac{E_e}{mc^2}\right)^2\frac{heB(r)\sin\theta}{mc}$$

is the characteristic energy, $B(r) = B_*(R_*/r)^3$, R_* and B_* are the radius and magnetic field on the neutron star surface, respectively, and $F(x) = x\int_x^\infty K_{5/3}(t)\,dt$, where $K_{5/3}(t)$ is the modified Bessel function of order 5/3 (Blumenthal & Gould 1970). Then the spectrum of inverse Compton scattering is

$$F_{\rm ICS}(E_\gamma) = \int_{E_{\rm min}}^{E_{\max}}\frac{dN(E_e)}{dE_e}\left(\frac{d^2N_{\rm ICS}}{dE_\gamma\,dt}\right)dE_e , \quad (27)$$

where

$$\frac{d^2N_{\rm ICS}(E_\gamma, E_e)}{dE_\gamma\,dt} = \int_{\epsilon_1}^{\epsilon_2} n_{\rm syn}(\epsilon)F(\epsilon, E_\gamma, E_e)\,d\epsilon , \quad (28)$$

$$F(\epsilon, E_\gamma, E_e) = \frac{3\sigma_{\rm T}c(mc^2)^4}{16(E_e)^4\epsilon^2}\left\{2E_\gamma\ln\left[\frac{E_\gamma(mc^2)^2}{4E_e^2\epsilon}\right] + E_\gamma + \frac{4E_e^2\epsilon}{(mc^2)^2} - \frac{E_\gamma^2(mc^2)^2}{2E_e^2\epsilon}\right\} , \quad (29)$$

$$n_{\rm syn}(\epsilon) = \frac{F_{\rm syn}(\epsilon)}{cr^2\Delta\Omega} , \quad (30)$$

where E_γ is the photon energy, $n_{\rm syn}(\epsilon)$ is the photon density (with energy ϵ), $F_{\rm syn}(\epsilon)$ is the calculated synchrotron radiation flux, and $\Delta\Omega$ is the solid angle of the fan beam. For simplicity, we will assume $\Delta\Omega \sim 1$ sr.

5. CALCULATED RESULTS AND DISCUSSIONS

In general, there are three parameters in this model, namely, the size of the outer gap (f), the mean distance to the outer gap ($r = \beta r_L$), and the power index of energy distribution of the electron/positron pairs. However, we can assume that the inclination angles of the Crab-type pulsars are similar, so that this parameter can be fixed by a self-consistency requirement (cf. note b in Table 2). Furthermore, if there are very few further generations of electron/positron pairs in the magnetosphere, then the power index is 2; otherwise, it should be close to 3. With these two assumptions, our model only contains one free parameter f. In practice, f is not easy to determine uniquely, unless the upper energy cutoff is known. However, the Crab pulsar does have this information, so its f is unique. For other pulsars, we will use equation (4) to estimate f by comparison with the Crab pulsar. The estimated f and other relevant parameters for these six pulsars with unusually intense X-ray emission are shown in Table 2.

TABLE 2

CALCULATED PARAMETERS OF SIX CRAB-TYPE PULSARS

PSR	log τ	f[a]	β[b]	$E_{\max}$[c]	$E_{\min}$[d]
Crab	3.1	0.1	0.78	1500	1.1
0540−69.....	3.2	0.17	1.4	2000	0.511
1509−58.....	3.2	0.5	0.13	4500	0.511
1823+13.....	4.5	0.52	0.13	4600	0.511
2334+61.....	4.7	4.7	0.09	1700	0.511
1951+32.....	5	0.78	0.11	2900	0.511

[a] f is calculated from eq. (4).
[b] β is obtained self-consistently by $\int_{E_{\rm min}}^{E_{\max}}\dot{E}_e(dN/dE_e)\,dE_e = e\dot{N}\Delta V$.
[c] $E_{\max}$ is calculated from eqs. (17) and (3).
[d] $E_{\rm min}$ is obtained from equation (25).

5.1. *The Crab*

We have chosen $f = 0.1$ such that the spectral break occurs at $\sim$ MeV (Ulmer et al. 1993; Ulmer 1994). This choice of f also gives a correct upper energy cutoff at ~ 10 GeV (Thomson et al. 1993) and a correct phase separation ($\Delta\phi$) of the double pulse (if $\beta = 0.78$, $\Delta\phi$ is 140°–220°; cf. Fig. 9 of CHR II). Figure 1 shows the comparison between the model spectra and the observed data. The spectral index of $e^{\pm}$ pairs is 2.8 instead of 2 because the crossed beam emission geometry of the outer gap model (cf. Fig. 7 of CHR II) will result in additional pair production, which modifies the emitting particle distribution. Further generations of pairs, e.g., tertiary pairs or even higher, should be considered in the emission processes. For the parameters of the Crab pulsar, these further generations, indeed, play an important role. The detailed calculation of the γ-ray spectrum of the Crab spectrum can be found elsewhere (e.g., CHR II; Ho 1989; Romani & Chiang 1994). Nevertheless, our simple model indeed provides a consistent description for the emission spectrum of the Crab pulsar.

5.2. *PSR 0540−69*

Figure 2 shows that the spectral index if $e^{\pm}$ pairs is 2 and that the inverse Compton component is not significant for all possible values of f, except those much larger than the scaled value from that of the Crab pulsar (cf. eq. [4]). This suggests that, the optical depth of this pulsar is not as large as that of the Crab pulsar, so further generations of pairs have not been produced. This result is also consistent with the fact that the magnetospheric volume of this pulsar is about $(\Omega_{\rm Crab}/\Omega_{0540})^3 \sim 4$ times that of the Crab pulsar.

5.3. *PSR 1509−58*

The f of PSR 1509−58 scaled from that of the Crab (eq. [4]) seems to fit the observed results of *ROSAT* and OSSE and is also quite consistent with the upper limits of *COS B* and EGRET (see Fig. 3). The inferred mean distance to the outer gap is $\beta r_L \sim 0.15 r_L$, which implies that the phase separation between two pulses is less than 90°. Such a small phase separation results in a single broad pulse which is consistent with the observed light curve. We want to remark that the parameters of this pulsar, namely, its magnetic field and period, suggest that it can be either a Crab-type pulsar or a Vela-type pulsar depending on its actual inclination angle (the classification of Vela-type pulsars and Crab-type pulsars; cf. Cheng & Ding 1994). For a very small inclination angle, the mean distance to the outer gap can approach the light cylinder radius. The smaller B field makes the Vela-type mechanisms more favorable. Cheng & Ding (1994) assume that this pulsar is Vela-type and fit the observed spectrum by treating both f and β as free parameters. They obtain $f = 0.5$ and $\beta = 1.2$, respectively. Although the spectral fit of their model is as good as ours, the value of β seems too large. So we believe that PSR 1509−58 should be a Crab-type pulsar rather than a Vela-type.

5.4. *PSR 1951+32*

If f is close to the value predicted by equation (4), we expect that OSSE or COMPTEL may detect a signal from this pulsar and that the light curve should be a single broad beam. See Figure 4.

5.5. *PSR 1823−13*

Again, if equation (4) does work, we expect that OSSE and COMPTEL should have a better chance of detecting a γ-ray signal from this pulsar than EGRET. Again, the light curve should be a single broad beam. See Figure 5.

5.6. *PSR 2334+61*

The scaling model for this pulsar seems to fail because the predicted f is larger than unity (see Fig. 6). There are two possibilities. First, the inclination angle of this pulsar may be substantially larger than that of the Crab pulsar. In this case,

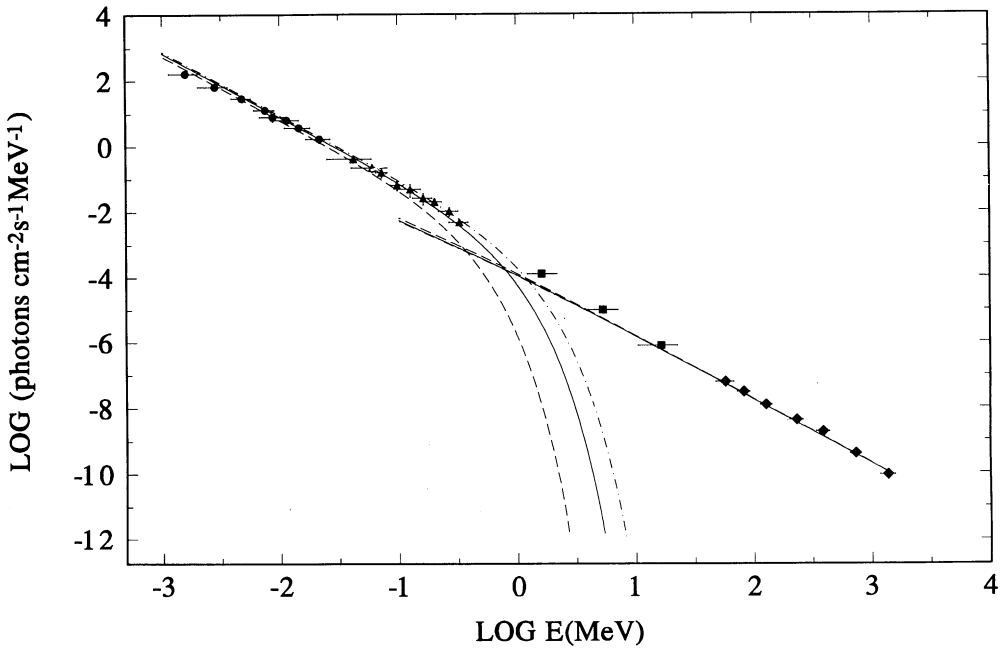

FIG. 1.—Calculated and observed photon spectra of the Crab pulsar. The dot-dashed line, solid line, and dashed line correspond to $f = 0.02$, 0.1, and 0.08, respectively. The solid circles are the combined data from Fritz et al. (1971), Toor & Seward (1977), and Prado & Serlemitsos (1981). The solid triangles are from OSSE (Ulmer et al. 1993; Ulmer 1994). The solid squares are from COMPTEL (Nolan et al. 1993). The solid diamonds are from EGRET (Thompson et al. 1993).

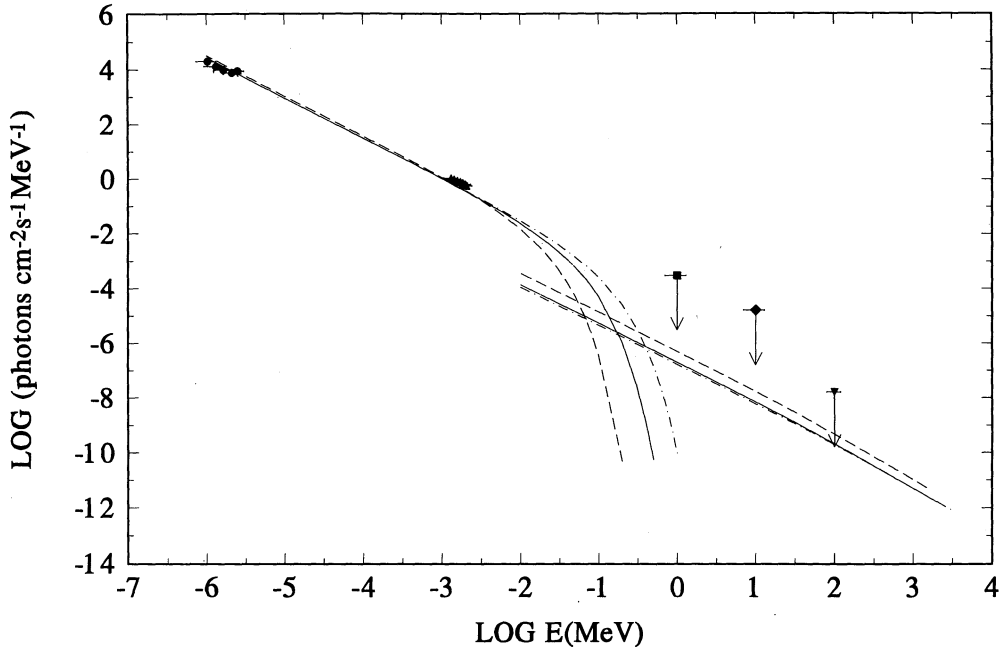

FIG. 2.—Calculated and observed photon spectra of PSR 0540−69. The dot-dashed line, solid line, and dashed line correspond to $f = 0.2$, 0.17, and 0.14, respectively. The solid circles are optical data (Middleditch, Pennypacker, & Burns 1987). The solid triangles are the X-ray data from *ROSAT* (Finley et al. 1993). The solid square, diamond, and inverted triangle are the upper limits of OSSE, COMPTEL, and EGRET, respectively.

the phase separation of two γ-ray beams should be 180° because this pulsar is expected to be near orthogonal rotation. The second possibility is that the "unusually" intense X-ray emission may result from a recent glitch (cf. Chong & Cheng 1993). If that is the case, it also implies that this pulsar will have a very unusual braking index (Cheng, Chong, & Lee 1994).

We would like to make three remarks. First, the size of the outer gap (f) gradually increases with age (cf. Table 2). This seems to agree qualitatively with the pulsar evolution model (Ruderman & Cheng 1988). Second, pulsars more than 10^4 yr old (e.g., the Vela pulsar) are expected to behave like Vela-type pulsars which emit very little X-rays. However, we want to point out that if the inclination angle of the pulsar is sufficiently large such that the mean magnetic field of the outer gap is as

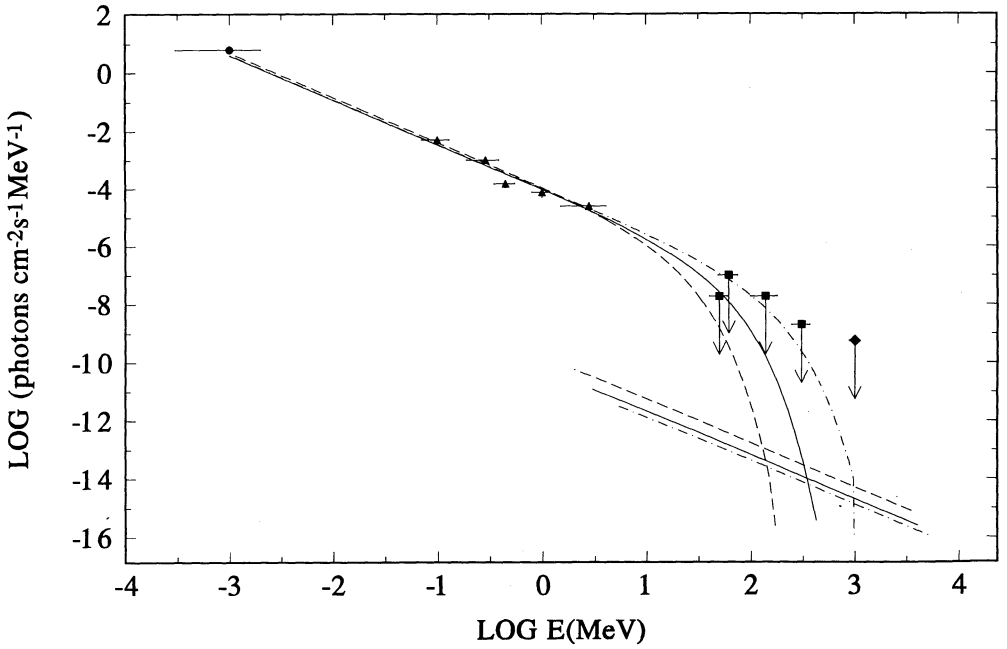

FIG. 3.—Calculated and observed photon spectra of PSR 1509−58. The dot-dashed line, solid line, and dashed line correspond to $f = 0.6$, 0.5, and 0.4, respectively. The solid circle is the *ROSAT* data (cf. Ögelman 1993). The solid triangles are data from OSSE (Matz et al. 1994). The solid square and the diamond are the upper limits of *COS B* (Brazier et al. 1993) and EGRET (Hartmann et al. 1993).

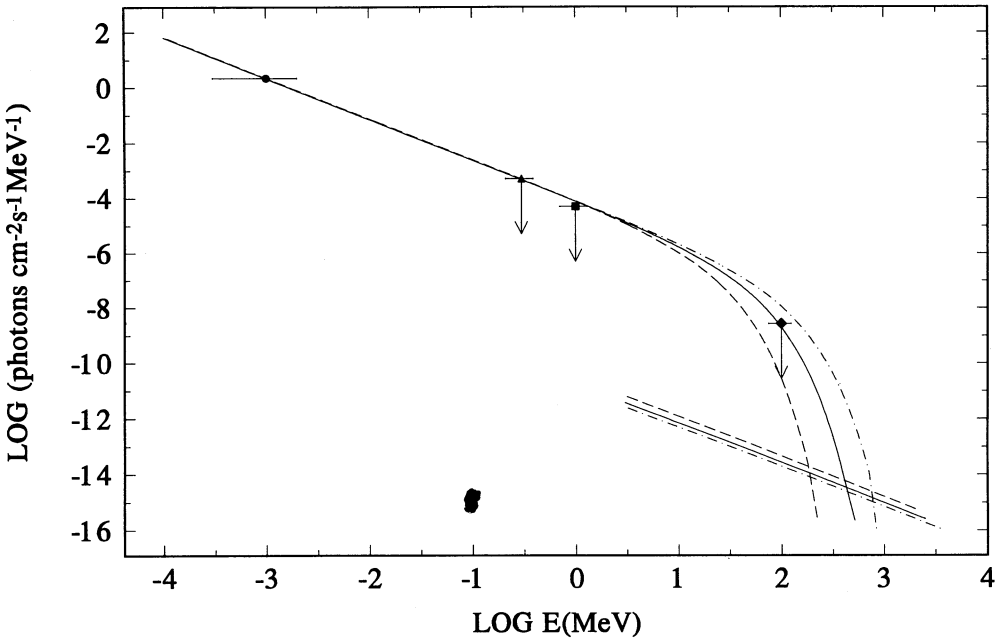

FIG. 4.—Calculated and observed photon spectra of PSR 1951+32. The dot-dashed line, solid line, and dashed line correspond to $f = 0.93$, 0.78, and 0.62, respectively. The solid circle is the *ROSAT* data (cf. Ögelman 1993). The solid triangle, square, and diamond are the upper limits of OSSE, COMPTEL, and EGRET, respectively.

strong as that of the Crab pulsar, the radiation and pair-production mechanisms of this pulsar can mimic those in the Crab pulsar. Third, the inferred β from f can give information on the phase separation between two pulses.

In summary, we have used the observed X-ray results to select six pulsars which show unusually intense X-ray emission, higher than that predicted by theoretical models. Since the key consequence of the Crab-type radiation mechanisms is X-ray emission, we therefore assume that these pulsars are Crab-type pulsars. We have used simple synchrotron self-Compton mechanisms to calculate the model X-ray and γ-ray spectra and we have compared them with the observed results and upper limits. Our model parameters and spectra may provide useful information for future observations.

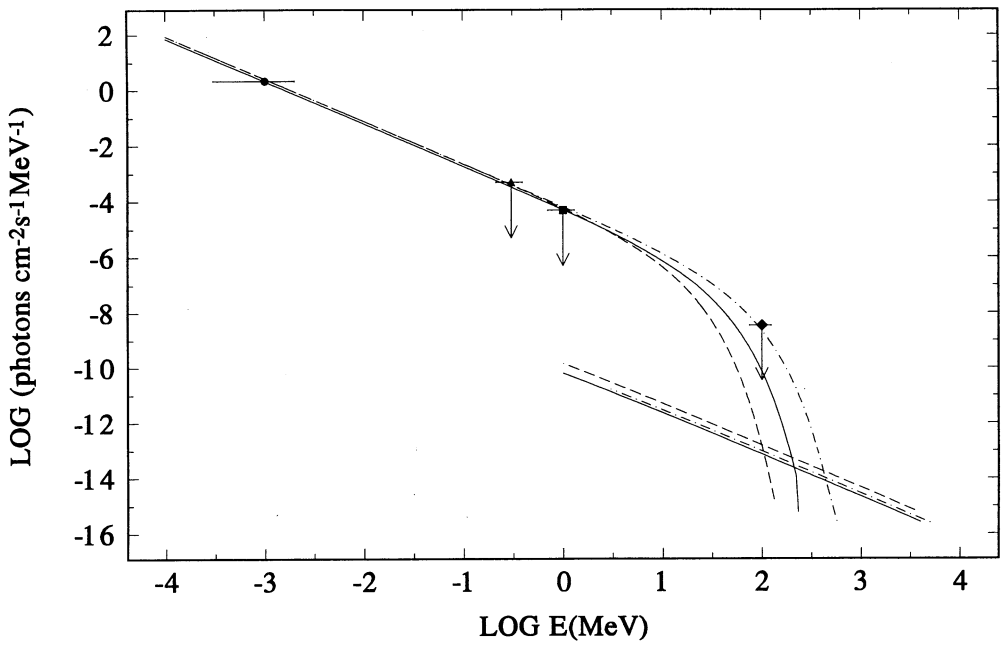

FIG. 5.—Calculated and observed photon spectra of PSR 1823−13. The dot-dashed line, solid line, and dashed line correspond to $f = 0.62$, 0.52, and 0.42, respectively. The solid circle is the *ROSAT* data (cf. Ögelman 1993). The solid triangle, square, and diamond are the upper limits of OSSE, COMPTEL, and EGRET, respectively.

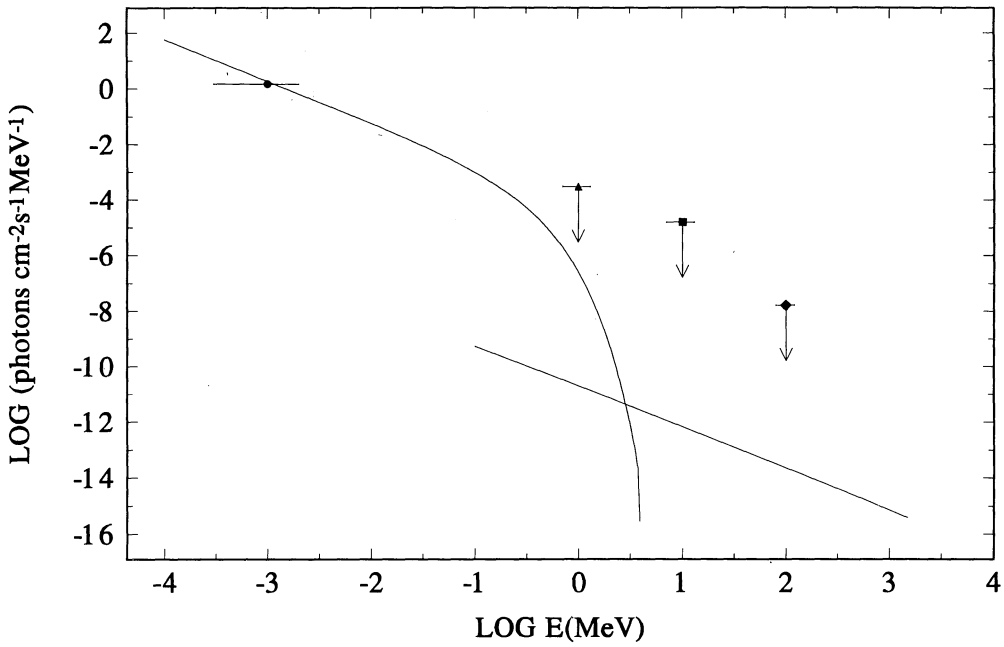

FIG. 6.—Calculated and observed photon spectra of PSR 2334+61. The solid line corresponds to $f = 1$. The solid circle is the *ROSAT* data (cf. Ögelman 1993). The solid triangle, square, and diamond are the upper limits of OSSE, COMPTEL, and EGRET, respectively.

REFERENCES

Alpar, M. A., Anderson, P. W., Pines, D., & Shaham, J. 1984, ApJ, 276, 325
Alpar, M. A., et al. 1987, A&A, 177, 101
Alpar, M. A., Chau, H. F., Cheng, K. S., & Pines, D. 1993, ApJ, 409, 345
———. 1994, ApJ, 427, L29
Arons, J., & Scharleman, E. T. 1979, ApJ, 231, 854
Baym, G., Pethick, C. J., & Sutherland, P. 1971, ApJ, 170, 299
Baym, G., & Pines, D. 1971, Ann. Phys., 66, 816
Becker, W., & Trümper, J. 1993, Nature, 365, 528
Bertsch, D. L., et al. 1992, Nature, 357, 306
Bluementhal, G. R., & Gould, R. J. 1970, Rev. Mod. Phys., 42, 237
Brazier, K. T. S., et al. 1994, MNRAS, 268, 517
Chen, K., & Ruderman, M. A. 1993, ApJ, 402, 624
Cheng, K. S. 1994, Proc. Towards a Major Atmospheric Cherenkov Detector III for TeV Astro/Particle Physics, ed. T. Kifune (Tokyo: Universal Academy), 25
Cheng, K. S., Chau, W. Y., Zhang, J. L., & Chau, H. F. 1992, ApJ, 396, 135
Cheng, K. S., Chong, N., & Lee, T. M. 1994, ApJ, 434, 733
Cheng, K. S., & Ding, W. K. Y. 1994, ApJ, 431, 724
Cheng, K. S., Ho, C., & Ruderman, M. 1986a, ApJ, 300, 500 (CHR I)
———. 1986b, ApJ, 300, 522 (CHR II)
Chong, N., & Cheng, K. S. 1993, ApJ, 425, 210
De Jager, O. C., & Harding, A. K. 1992, ApJ, 396, 161
Epstein, R. I., & Baym, G. 1988, ApJ, 328, 680
Fierro, J. M., et al. 1993, ApJ, 413, L27
Finley, J. P., Ögelman, H., Hasinger, G., & Trümper, J. 1993, ApJ, 410, 323
Fritz, G., et al. 1971, ApJ, 164, L55
Gould, R. J. 1965, Phys. Rev. Lett., 15, 577
Gudmondson, E. H., Pethick, C. J., & Epstein, R. I. 1982, ApJ, 272, 286
Halpern, J., & Ruderman, M. A. 1993, ApJ, 415, 286
Harding, A. K. 1981, ApJ, 245, 267
Hartmann, D. H., Brown, L. E., Clayton, D. D., Schnepf, N., Cords, J. M., & Harding, A. 1993, in Proc. Los Alamos Workshop on Isolated Pulsars, ed. K. A. Van Riper, R. Epstein, & C. Ho (Cambridge: Cambridge Univ. Press), 405
Ho, C. 1989, ApJ, 342, 396
Kennel, C. F., & Coroniti, F. V. 1984, ApJ, 283, 694
Mattox, J. R., Bertsch, D. L., Fichtel, C. E., Hartman, R. C., Kniffen, D. A., & Thomson, D. J. 1992, ApJ, 401, L23
Matz, S. M., et al. 1994, ApJ, 434, 288
Middleditch, J., Pennypacker, C. R., & Burns, M. S. 1987, ApJ, 315, 142
Nolan, P. L., et al. 1993, ApJ, 409, 697
Ögelman, H. 1993, in Lives of Neutron Stars, ed. M. A. Alpar, Ü, Kiziloglu, J. Van Paradijs (Dordrecht: Kluwer)
Pandharipande, V. R., Pines, D., & Smith, R. A. 1976, ApJ, 208, 550
Prado, S. H., & Serlemitsos, P. J. 1981, ApJ, 246, 484
Rieke, G. H., & Weekes, T. C. 1969, ApJ, 15, 577
Ruderman, M. A. 1991, ApJ, 366, 213
Ruderman, M. A., & Cheng, K. S. 1988, ApJ, 335, 306
Ruderman, M. A., & Sutherland, P. 1975, ApJ, 196, 51
Romani, R., & Chiang, J. 1994, ApJ, 436, 754
Scharlemann, E. T., Arons, J., & Fawley, W. M. 1978, ApJ, 222, 297
Shibaziki, N., & Lamb, F. 1989,ApJ, 346, 808
Strickman, M. S., et al. 1993, in AIP Conf. Proc. 280, *Compton Gamma-Ray Observatory*, ed. M. Friedlander, N. Gehrels, & D. Macomb (New York: AIP), 209
Taylor, J., Manchester, R., & Lyne, A. 1993, ApJS, 88, 529
Thompson, D. J., et al. 1992, Nature, 359, 615
———. 1993, in Proc. Los Alamos Workshop on Isolated Pulsars, ed. K. A. Van Riper, R. Epstein, & C. Ho (Cambridge: Cambridge Univ. Press), 230
Toor, A., & Seward, F. D. 1977, ApJ, 216, 560
Ulmer, M. P. 1994, ApJS, 90, 789
Ulmer, M. P., et al. 1993, ApJ, 417, 738
Ulmer, M. P., & Schroeder, P. C. 1994, preprint
Wilson, R. B., Finger, M. H., Fishman, G. J., Meegan, C. A., & Paciesas, W. S. 1992, IAU Circ. 5429
Wilson, R. B., et al. 1993, in Proc. Los Alamos Workshop on Isolated Pulsars, ed. K. A. Van Riper, R. Epstein, & C. Ho (Cambridge: Cambridge Univ. Press), 257
Wiringa, R. B., & Fiks, V. 1988, Phys. Rev. C, 38, 1010